Thermochemical energy storage using the phase transitions brownmillerite-2H perovskite-cubic perovskite in the $Ca_xSr_{1-x}CoO_{3-\delta}$ (x=0 and 0.5) system

M. Teresa Azcondo[†]*, María Orfila[l], María Linares[l], Raúl Molina[‡], Javier Marugán[‡], Ulises Amador[†], Khalid Boulahya[⁑], Juan Ángel Botas[l], Raúl Sanz[‡]*

[†] San Pablo-CEU University, CEU Universities, Pharmacy Faculty, Chemistry and Biochemistry Department, Montepríncipe Urbanization, Boadilla del Monte, E-28668, Madrid, Spain.

[l] Chemical, Energy and Mechanical Technology Department, Rey Juan Carlos University, Tulipán, s/n, E-28933, Móstoles, Spain.

[‡] Chemical and Environmental Technology Department, Rey Juan Carlos University, Tulipán, s/n, E-28933, Móstoles, Spain.

[⁑] Inorganic Chemistry Department, Chemistry Faculty, Complutense University, E-28040 Madrid, Spain.

KEYWORDS: thermochemical energy storage, perovskite, brownmillerite, cyclability, thermal hysteresis, structural transition, redox processes.

ABSTRACT

The oxides $Ca_{0.5}Sr_{0.5}CoO_{3-\delta}$ and $SrCoO_{3-\delta}$, which present perovskite or perovskite-related phases in different temperature domains, have been tested as materials for thermochemical energy storage. The first one, $Ca_{0.5}Sr_{0.5}CoO_{3-\delta}$, experiences a reversible phase transition upon consecutive cycles under air flow at a maximum operating temperature of 1196 K. Unfortunately, the heat stored in this process, associated to an oxygen loss/gain and a structural phase transition, is very small hindering its use for thermochemical heat storage. The as-prepared oxide $SrCoO_{3-\delta}$, which displays a brownmillerite structure like the Ca-containing compound, in the first heating step irreversibly segregates some Co_3O_4 at 823 K to yield a 2H hexagonal-perovskite. This phase reversibly transforms at 1073 K into a cubic-perovskite. These $2H \rightleftarrows C$ transition occurs from the second to, at least, thirty cycles. The average absorbed and released heat are ~104.1±0.06 J/g and ~68.8±1.8 J/g, respectively, and therefore $SrCoO_{3-\delta}$ presents a high exo/endo ratio. The exergy efficiency is, on average for the 30 cycles performed, as high as 63.9±1.2%. The mechanism of the phase $2H \rightleftarrows C$ transition of $SrCoO_{3-\delta}$ explains the good performance of this material for thermochemical energy storage.

INTRODUCTION

The world energy demand grows every year, and thus the CO_2 emissions with the consequent environmental problems. The search for new energy alternatives environmentally friendly is one of the main concerns in the current century. In this context, renewable energy sources are becoming more important.[1] Among them, the radiation coming from the sun is the most abundant.[2] Solar

radiation can be used through three different well-defined concepts: thermal, photovoltaics (PV), and concentrated solar power (CSP). The first one is focused on domestic applications in which solar energy is generally used as a heat source at low temperature (< 373 K). PV and CSP technologies are focused mainly on electricity production at different scales. However, the use of this type of energy implies a challenge in the development of storage technologies to overcome the limitations associated with the discontinuous nature of this energy source and achieve continuous 24 h electricity production.[3,4] CSP has an important advantage due to the possibility of combining the solar field with Brayton-Rankine conventional thermodynamic cycles. Additionally, CSP plants allow implementing efficient thermal energy storage (TES) systems. The excess heat collected by the solar field can be stored via three different TES approaches: sensible, latent, and thermochemical heat processes. [5,6]

Nowadays, sensible heat systems based on molten salts are the only commercially available TES technology in large-scale CSP plants.[5] However, the salts usually present stability problems due to the high working temperatures (723 K-838 K). Additionally, considerable amounts of salts are required, due to their low energy density, and the installations must be large and complex due to the nature of the energy-storage mechanism; both factors imply an increase in the capital cost of the CSP plants. Apart from this, corrosiveness, exergy destruction due to temperature gradients between room-temperature and the working temperature, and the risk of solidification owing to the high melting temperatures of common salts are the main disadvantages of current molten-salt systems.[7-9]

Latent heat TES systems can reach higher efficiencies than sensible heat TES systems due to their nearly isothermal operational conditions. However, despite the huge number of phase-change materials (PCMs) proposed in the literature,[10, 11] they are not yet available for large CSP plants

because of their low charge/discharge rates derived from the low thermal conductivity of most PCMs, solid deposition on heat transfer surfaces and large volumetric variations associated with the phase change.[12, 13]

On the contrary, thermochemical energy storage (TCES) systems have a great potential for future CSP plants thanks to the large energy density of the materials employed and high operational temperatures, increasing the efficiency of steam turbines.[14, 15] TCES systems imply the utilization of reversible chemical reactions (Equation 1) to store thermal energy. The solar energy collected in the CSP plant is used to carry out an endothermic reaction to store it in the chemical bonds of the products. Then, when the heat is needed in off-sun periods, the reverse exothermic reaction is carried out, releasing the heat stored.[16]

$$A + \Delta H_r \rightleftarrows B + C \tag{1}$$

So, the energy stored is proportional to the molar enthalpy of reaction (ΔH_r). The requirements for TCES materials are: reversibility of the chemical reactions, temperatures compatible with power cycles, high reaction rates, absence of side reactions, high specific enthalpy of reaction, high specific heat capacity, long-term cycling stability, environmental compatibility, and low cost.[17] A huge number of reactions and materials have been investigated for their application in TCES systems such as NH_3, CH_4, SO_3, MCO_3, MH, $M(OH)_2$, where M denotes a metal element.[5, 6, 18, 19] In the recent decades, the TCES research is mainly focused on redox processes (Equation 2) based on metal oxides through their redox reversibility, higher operational temperatures, as compared to molten salts, and absence of product gases that require separation.[16] In these processes, the charge is the endothermic solar-driven reduction. Heat is required for the reduction of a metal oxide,

4

which results in a metal oxide with a lower oxidation state and the release of lattice oxygen to the ambient. When energy is needed, the discharge is performed oxidizing the reduced metal oxide with ambient air, releasing the stored energy owning to the exothermic nature of this oxidation reaction.

$$MeO_x\,(s) + \Delta H_r \rightleftarrows MeO_{x-y}(s) + \frac{y}{2}O_2(g) \tag{2}$$

Different metal-oxygen systems (oxides and peroxides) such as BaO_2/BaO, CuO/Cu_2O, Fe_2O_3/FeO, ZnO/Zn, Co_3O_4/CoO, and Mn_2O_3/MnO have been studied for this application. However, they present noticeable limitations associated with the lack of cyclability, the high required temperatures, and the slow kinetics. In the aforementioned cases, the oxidation/reduction processes are accompanied by a severe atomic re-arrangement, since the structure of the oxidized and reduced phases are totally different.[20] The system Co_3O_4/CoO is the most promising one for TES application, however the cost and toxicity of cobalt is a serious drawback. New materials are needed for application in real TES devices.[20] To overcome these issues, new systems based on mixtures of cobalt oxide with oxides of cheap and safe metals have been proposed.[18] More recently, blends of oxides of metals as iron and manganese, have been reported, displaying good performances in terms of energy storage capacity and durability.[21]

As an alternative, perovskites have been recently proposed for thermochemical energy storage (Equation 3) as they are stable in a large range of oxygen non-stoichiometry and temperatures, showing no phase transition ensuring good cyclability. Besides, many of them present high electronic and/or ionic conductivity that may extend the reaction given in Equation 3 to the bulk of the material, increasing the mass involved in the process and improving the kinetics.[22-27]

$$ABO_{3-\delta}\,(s) + \Delta H_r \rightleftarrows ABO_{3-\delta-y}(s) + \frac{y}{2}O_2(g) \tag{3}$$
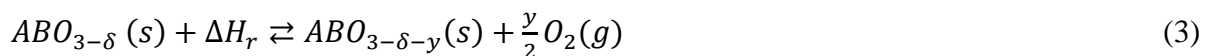
Materials presenting a compromise between those extreme behaviors: a) deep atomic rearrangement in the phase transition with high specific energy associated but with slow kinetics and poor reversibility, and b) a redox process with no phase transition associated and good reversibility and fast kinetics; will be good candidates for TCES. As suggested by Vieten et al. [28] the use of phase transitions induced or coupled with redox processes could be beneficial for thermochemical energy. Some metal oxides display a reversible phase transition associated with a redox process driven by oxygen release or gain, like those studied in the present work.

Thus, the present study aims to explore some oxides with perovskite-related structure, $Ca_xSr_{1-x}CoO_{3-\delta}$ (x=0 and 0.5) system, as TCES materials, taking advantage of the coupling of oxygen release/metal reduction and a structural transition. It is known that many oxides of composition $(AE)MO_{3-\delta}$ (AE = Alkaline-Earth, M=3d metal) experience loss/gain of oxygen as a function of temperature and oxygen partial pressure, and in many cases this redox process is associated to structural phase transitions. These may involve only the ordering/disordering of oxygen vacancies (brownmillerite-to-perovskite) or may involve the re-arrangement of metal ions (2H-to-perovskite), as well. The title compounds are examples of these two cases: $Ca_{0.5}Sr_{0.5}CoO_{3-\delta}$ of the former, and $SrCoO_{3-\delta}$ of the latter.

These examples provide a guideline to the design of new TCES materials in which the redox process is associated with any other reversible transition, either structural, magnetic, or electric, which may improve the performance of the materials.

MATERIALS AND METHODS

Samples preparation. The title materials, $SrCoO_{3-\delta}$ and $Ca_{0.5}Sr_{0.5}CoO_{3-\delta}$ (denoted as SCO and CSCO, respectively) have been synthesized in a two-step procedure. Precursors have been obtained by a solution-combustion method using $Sr(NO_3)_2$, $CaCO_3$, and $Co(NO_3)_2 \cdot 6H_2O$ as metal sources and oxidizing agent and glycine as fuel; all chemicals from Sigma-Aldrich with a purity of 99.95 % were used as received. The combustion reaction was carried out in chemically stoichiometric water solutions with balanced oxidizer-to-fuel ratio.[29] Combustion of these solutions is induced by heating them into a muffle furnace, pre-heated at 773 K, for half an hour. These precursors have been homogenized and grounded by hand in a mortar. Different thermal treatments have been applied for the two compositions to obtain single-phase brownmillerite (B) samples. Thus, to obtain $B-SrCoO_{3-\delta}$ (B-SCO) the precursor powder is fired in air at 1423 K for 12 hours and quenched in liquid nitrogen from this temperature. The Ca-containing brownmillerite ($B-Ca_{0.5}Sr_{0.5}CoO_{3-\delta}$, denoted as B-CSCO) has been prepared by heating the corresponding precursor in air at 1373 K for 12 hours slowly cooled by turning the furnace off.

Structural and microstructural characterization. The purity of the as-prepared samples has been determined by X-ray diffraction (XRD) at room temperature (RT) on a Bruker D8 high-resolution diffractometer equipped with a LynxEye® fast detector using monochromatic CuKα1 ($\lambda = 1.5406$ Å) radiation obtained with a germanium primary monochromator. The angular range, step size, and counting times were selected to reach enough data quality and resolution for phase refinements. Diffraction data were analyzed by the Rietveld method using Fullprof software.[30]

X-ray diffraction patterns at different temperatures in the 298–1273 K range were taken every 50 K in air with stabilization for 30 min, applying a heating/cooling rate of 2 K min-1 on a Multi-Purpose PANalyticalX'Pert PRO MPD diffractometer using CuKα ($\lambda = 1.5418$ Å) radiation and

equipped with an Anton Paar HTK2000 camera. The diffraction patterns were analyzed by the LeBail method [31] using the Fullprof software.[30]

The samples have been further characterized by electron diffraction and high-resolution electron microscopy (HREM) using a Jeol 3000 FEG electron microscope, equipped with a double tilting goniometer stage ($\pm 20°$, $\pm 20°$).

Thermogravimetric measurements. The evaluation of the activity of the materials was performed by thermogravimetric analysis (TGA) using a TGA/DSC1 STARe System (Mettler, Toledo) with a maximum temperature operation of 1873 K. Different consecutive cycles were performed to evaluate the re-oxidation capacity of the materials under air flow (100 cm^3/min). The samples (50 mg) were placed in an alumina crucible of 0.15 cm^3 of total volume. The samples were heated up from room temperature to 1273 K with a heating rate of 10 K/min.

RESULTS AND DISCUSSION

Samples purity and room temperature structures. Figures S1 and S2 display the result of fitting the RT XRD patterns corresponding to the B-SCO and B-CSCO samples used in this study to the structural models given in Table S1. Both samples are single-phase with average brownmillerite-like structure. Since the oxygen X-ray scattering power is low compared to those of the metal atoms present in these compounds, the exact anion content cannot be obtained from the diffraction data; on the contrary, the metal contents have been confirmed to be the nominal ones. In any case, TGA analyses (Figures S3 and S4) indicate that the phases are $SrCoO_{2.50}$ and $Ca_{0.5}Sr_{0.5}CoO_{2.75}$, as discussed below.

The RT structure at the local level of $SrCoO_{2.50}$ has been studied by TEM and HRTEM, the orthorhombic symmetry and the $a_p\sqrt{2}\times4a_p\times a_p\sqrt{2}$ (where a_p refers to the perovskite cell parameter) unit cell have been confirmed. The most informative micrograph taken along [001] (Figure 1a) shows a well-ordered material with d-spacings of 5.4 Å and 15.4 Å, corresponding to d_{100} and d_{010}, respectively. The contrast observed in high resolution image highlights the expected order of brownmillerite-like structure where CoO_6 octahedra and CoO_4 tetrahedra layers successively stack in an ordered sequence along the b-axis. Different orientation of consecutive CoO_4 tetrahedra layers leads to 4ap distances along the b axis as observed on the experimental HRTEM picture shown in Figure 1a.
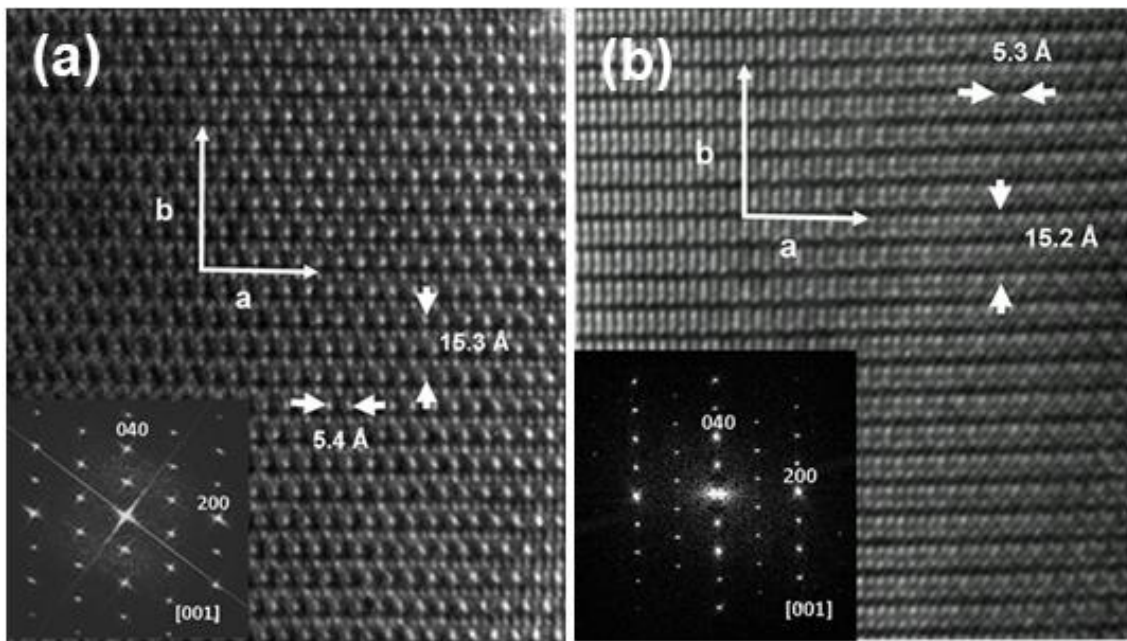

Figure 1. HRTEM micrographs brownmillerite-like compounds taken along [001] zone axis, (a) of $SrCoO_{2.5}$ and (b) $Ca_{0.5}Sr_{0.5}CoO_{2.75}$. The corresponding optical fast Fourier transforms of the images are shown in the insets.

The HRTEM micrograph for $Ca_{0.5}Sr_{0.5}CoO_{2.75}$, taken along the [001] zone axis (Figure 1b), shows a well-ordered material with d-spacings of 5.3 and 15.2 Å, corresponding to d_{100} and d_{010} of the above-described unit cell. The contrast variation is very similar to that of the non-substituted parent compound ($SrCoO_{3-\delta}$), with ordered stacking CoO_6 octahedra and CoO_4 tetrahedra layers characteristic of the brownmillerite structure.

Thermal evolution of the materials. Although the two materials studied adopt the same brownmillerite structure at RT, when heated in air flow they evolve in noticeably different manners.

The $SrCoO_{2.50}$ compound retains the brownmillerite structure up to 823 K as determined by XRD thermo-diffraction (Figure S5) and depicted in Figure 2. Between this temperature and 923 K, three phases coexist. In this temperature range, a complex process given in Equation 4 takes place. Indeed, as shown by the TGA data on Figure S3, no mass change occurs up to around 840 K. From this temperature up to 940 K, a large mass gain of 1.24 % is produced, this range corresponds to the field in Figure 2 where the process given by Equation 4 takes place. It is well established [32] that the oxygen content of $SrCoO_{3-\delta}$ samples quenched from high temperature to liquid nitrogen is very close to 2.50 per formula unit (pfu). Assuming this value for our sample, the oxygen content of the sample at the end of the reaction is 15.86 pfu. Thus, the brownmillerite structure transforms into a 2H perovskite with partial segregation of Co_3O_4 since the 2H phase presents a Co:Sr ratio of 5:6 instead of 1:1 in the brownmillerite one.[33,34] In the $2H-Sr_6Co_5O_{15}$ oxide, the cobalt oxidation state is higher than in the brownmillerite (about $Co^{+3.6}$ instead of $Co^{+3.0}$).[33,34] Thus, a noticeable oxygen gain must be produced for the phase transition to occur. The 2H perovskite may be non-stoichiometric and, depending on the synthesis procedure, the oxygen content varies;[35] assuming Co_3O_4 to be stoichiometric, the composition of the 2H phase produced in the transition is

$Sr_6Co_5O_{14.53}$. It is difficult to detect the segregated Co_3O_4 by XRD (though NPD allows to do it [33]), in our case, segregation was confirmed by HRTEM and TEM, not shown).

$$6\ SrCoO_{2.50} + 0.43\ O_2 \rightarrow Sr_6Co_5O_{14.53} + 1/3\ Co_3O_4 \tag{4}$$
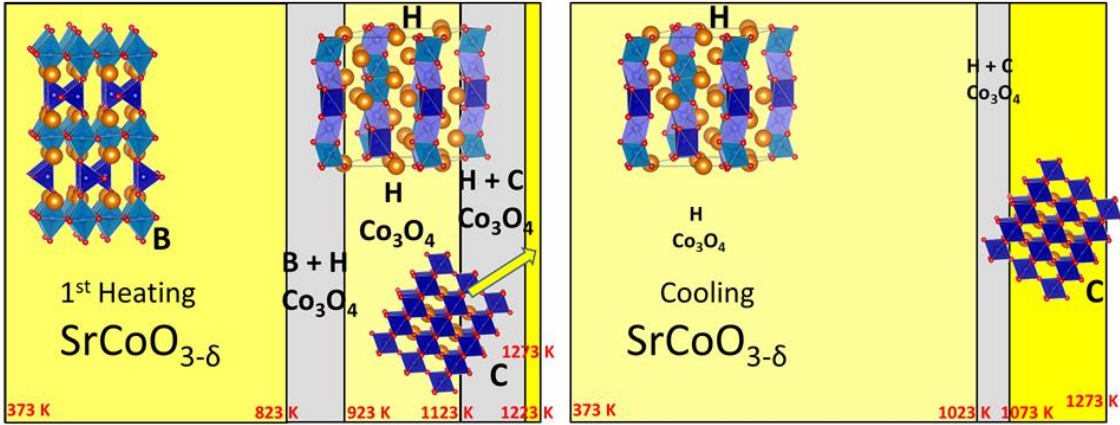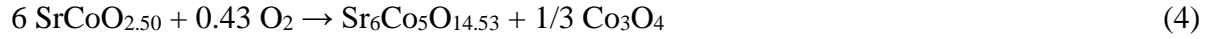

Figure 2. Temperature domains of the phases observed in the SCO sample on heating (left panel) and cooling (right panel).

Between 923 K and 1123 K, no phase transition occurs (Figure 2); the 2H-perovskite coexists with segregate Co_3O_4, but the brownmillerite phase disappears (Figure S5c). A continuous mass loss is observed in this temperature range (Figure S3); thus, the oxygen content of the 2H-phase at the end of this field is 13.99 pfu.

A second biphasic domain is observed in the range 1123 K–1223 K in which the 2H-perovskite transforms into a cubic perovskite (Figure S5d) with some oxygen loss (Figure S3) (in fact, three phases are present if one considers cobalt oxide). Above 1223 K, the only perovskite present is the cubic one (Figure S5e) with a composition $SrCo_{0.83}O_{2.26}$ (Figure S3).

On cooling, the SCO sample behaves in a noticeably different fashion. First, the stability field of the cubic perovskite expanded by 200 K, with a lower limit down to 1073 K (Figure S5f), though this could be a kinetic effect. In contrast, the biphasic C-2H domain slightly narrowed (1073 K– 1023 K). On cooling, C-perovskite gains oxygen (Figure S3), and this oxygen intake is accelerated when the 2H-perovskite starts to form. Interestingly, the oxygen content at 1023 K on cooling is almost the same as that on the heating cycle about 1123 K (the phase composition is $Sr_6Co_5O_{13.93}$), this suggests that the 2H structure needs a minimum oxygen stoichiometry corresponding to an oxygen content around 13.96(3) pfu and a minimum oxidation state of cobalt close to 3 (actually $Co^{+3.2}$).

Below 1023 K down to RT the only phase present (disregarding Co_3O_4, which plays no role in the phase transition 2H-perovskite $\rightleftarrows$ C-perovskite) is the 2H one (Figures S5g and S5h). On cooling down, the 2H-perovskite continuously gains oxygen down to 600 K. At this temperature, the maximum oxygen content is reached, so the composition of this phase is $Sr_6Co_5O_{14.70}$, and the cobalt oxidation state is $Co^{+3.48}$, in good agreement with what found for single crystals.[35] Thus, the most relevant difference between the heating and cooling steps is the disappearance of the brownmillerite phase from the phase-diagram.

When Sr is partially substituted for Ca, the obtained sample B-CSCO displays a phase diagram very different from that of the parent un-substituted $SrCoO_{2.50}$ oxide (Figure 3). In the heating stage, $Ca_{0.5}Sr_{0.5}CoO_{3-\delta}$ exists as a brownmillerite-like structure up to 1223 K (Figures S6a, S6b, and S6c). No 2H-perovskite is formed, nor does cobalt oxide segregation occur. Thus, partial substitution of Sr by Ca impedes the B→2H transition. The phase transition brownmillerite $\rightleftarrows$ cubic-perovskite is preceded by a large oxygen loss that takes place from 700 K up to 1223 K. Two plateaus are observed around 750 K and 1000 K. (Figure S4). A similar two-step mass loss

process has been reported for other members of the series $Ca_xSr_{1-x}CoO_{3-\delta}$.[36] These authors determined the oxygen content of the high-temperature phase to be very close to 2.50 pfu; with this assumption, the formula of the initial oxide is $Ca_{0.5}Sr_{0.5}CoO_{2.75}$, as stated above, whereas those of the two stable phases at intermediated temperatures evidenced in Figure S4 are: $Ca_{0.5}Sr_{0.5}CoO_{2.70}$ and $Ca_{0.5}Sr_{0.5}CoO_{2.54}$, respectively. The two weight losses observed are not associated with structural transitions, as the three phases display brownmillerite-like structure with different degrees of disordered anion vacancies (Figures S6a, S6b and S6c). A narrow real biphasic region exits, between 1223 K and 1273 K, where brownmillerite and cubic perovskite coexist. Beyond 1223 K a cubic perovskite is the only phase detected (Figure S6d).

In the cooling stage, the C-CSCO → B-CSCO transition occurs in a wide temperature range (Figure 3), (again the widening of the coexistence region may be due to kinetic reasons), between 1223 K and 973 K (Figures S6e, S6f, and S6g). Below this latter temperature, a stability field of the brownmillerite phase extends down to RT (Figures S6g and S6h). The large difference in oxygen contents between the pristine sample (2.75 oxygen pfu) and the one obtained on cooling (2.54 oxygen pfu) supports the slow kinetics of re-oxidation associated to the C-CSCO → B-CSCO transition.
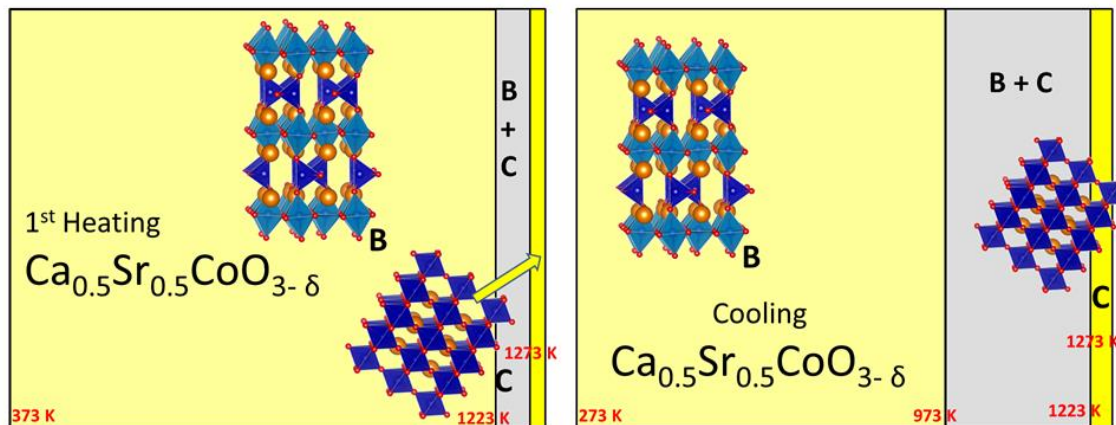
Figure 3. Temperature domains of the phases observed in the CSCO sample on heating (left panel) and cooling (right panel).

Study of cyclability. In the first heating-cooling cycle $SrCoO_{3-\delta}$ and $Ca_{0.5}Sr_{0.5}CoO_{3-\delta}$ samples experience very different structural and chemical changes, as a consequence, their behaviors from the second and consecutive cycles are noticeably different, as well. More importantly, the cyclability of the two samples from the second cycle is somewhat different, as Figure 4 shows. The details of the weight changes for the second cycle of both materials are depicted in Figures S7 and S8.

As depicted in Figure S7, for SCO, no mass change is observed up to 750 K; unlike what was observed for the pristine material in the first cycle (Figure S3), the sample loses oxygen continuously and uniformly up to 1185 K. This is most likely due to the creation of anion vacancies in the 2H-perovskite with composition $Sr_6Co_5O_{14.70}$ formed in the first cycle; the transition to the C-perovskite proceeds with a noticeable oxygen release (as observed in the first heating step) from a 2H-perovskite-like oxide with composition $Sr_6Co_5O_{13.93}$ to a $C\text{-}SrCo_{0.83}O_{2.26}$ phase. The cooling step in the second cycle is very similar to that of the first one; besides, all the released oxygen is recovered in a fully reversible process. The total weight reversibly released-recovered is about 1.8 %. The successive cycles (up to five) shown in Figure 4a are like the second one above described; thus, the first one can be considered as an activation step as observed in other systems.[37]
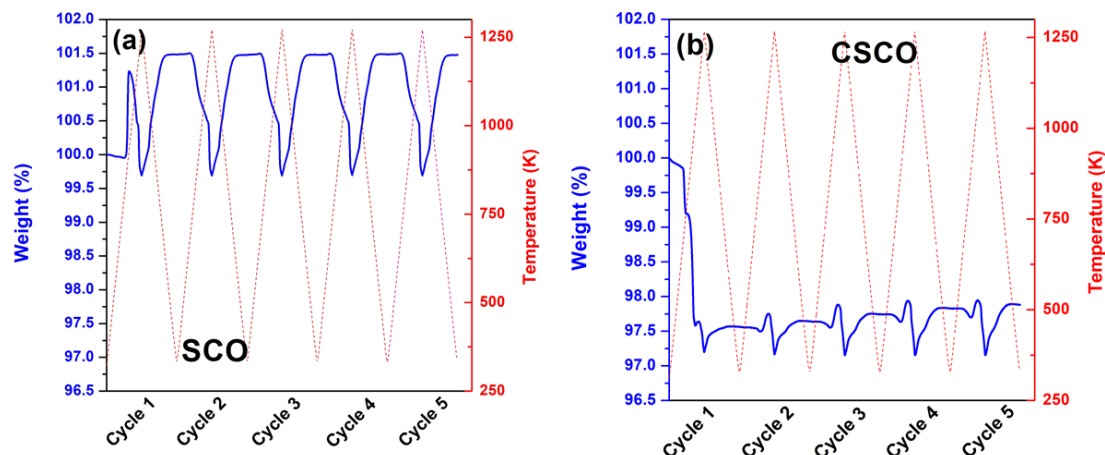
Figure 4. Weight variations upon cycling observed for a) SCO and b) CSCO.

The slow kinetics of oxygen gain/loss and reduction/oxidation of $Ca_{0.5}Sr_{0.5}CoO_{3-\delta}$ (CSCO), evidenced by the existence of a given phase in different temperature-domains in cooling and heating steps, plays a role in the materials cyclability. First, the material needs two cycles to be stabilized (Figure 4b), so to experience an almost stable mass variation of 0.73 % from the third cycle. However, as shown in Figure S8, the processes are not as reversible as they are for SCO (Figure S7). Assuming a composition $Ca_{0.5}Sr_{0.5}CoO_{2.50}$ at high temperature, the oxygen content at the beginning of the second cycle is 2.55 pfu, which is slightly higher than at the end of the first one (2.54 oxygen pfu). This is observed over the five cycles performed. As a result, at the end of the fifth cooling cycle, the oxygen content is 2.57 pfu, which is more than 1 % of extra oxygen with respect to the composition at the beginning of the second cycle. So, a progressive material re-oxidation takes place; it seems that the oxygen content at room temperature slowly tends to reach that of the pristine material (2.75 pfu, Figure S4).

Regarding the temperatures at which the reduction reaction begins (associated to oxygen loss) SCO requires about 750 K (Figure 4a and Figure S7) whereas for CSCO it is 700 K in the first

cycle but as high as 1100 K for the second and successive cycles (Figure 4b and Figure S8). These values are similar or even lower than those reported in the literature for other metal oxides commonly studied for this application,[38,39] which theoretically lead to higher efficiency of the solar collector system.[40] This is especially true for SCO with a low working temperature.

Study of the absorbed and released heat. The heat absorbed and released upon cycling was measured using the DSC of the TGA. In Figure 5, the results of five cycles for the SCO sample are shown.

From the second cycle, the heat flow displays good cyclability, in agreement with the good cyclability behavior of mass changes (Figure 4a). Two clear peaks are observed, an endothermic one at 1223 K and an exothermic one centered at 1013 K. On the contrary, in the first cycle (Figure 5b), another exothermic signal is observed at 883 K. Taking into account the information in Figures 3, S3, and S5 discussed above, this exothermic event corresponds to the structural phase transition brownmillerite → 2H-perovskite, which proceeds with the oxidation of cobalt associated to a noticeable oxygen gain and segregation of some Co_3O_4 (Equation 4). This process is irreversible, since the brownmillerite phase is not formed on cooling. The second, endothermic, peak observed in the first heating cycle can be ascribed to the 2H-perovskite → C-perovskite structural transition. This occurs with the reduction of cobalt due to a significant oxygen release (Figures 2, S3, and S5).

As the XRD thermo-diffraction revealed, in the first cooling, only one structural transition takes place between 1073 K–1023 K, which corresponds to the recovery of the 2H-perovskite phase with re-oxidation of cobalt by oxygen incorporation. As shown in Figure S3, the cubic perovskite experiences continuous and progressive oxidation as the temperature decreases from 1273 K. A

more pronounced oxygen gain is observed between 1070 K and 1023 K, temperature at which the

C → 2H transition is completed. As a result of the smooth nature of the re-oxidation process, the

exothermic peak centered at 1013 K is much broader than the corresponding endothermic one

(Figure 5b).

Since the B-phase is not recovered, during the rest of the cycles, the only active phase transition is

2H ⇄ C that is found to be highly reversible, not only in terms of mass change as shown in Figure

4a, but also from an energy point of view (Figure 5). Both aspects make this material a good

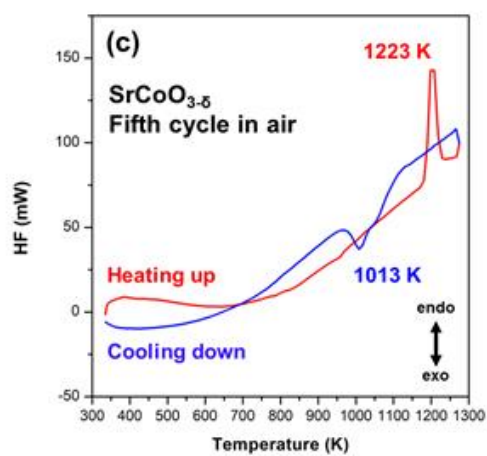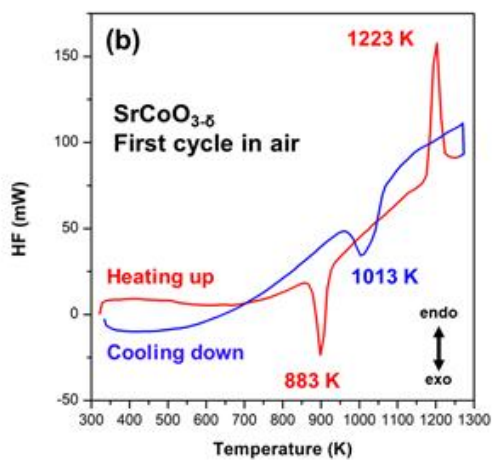candidate for thermochemical energy storage, as discussed below.
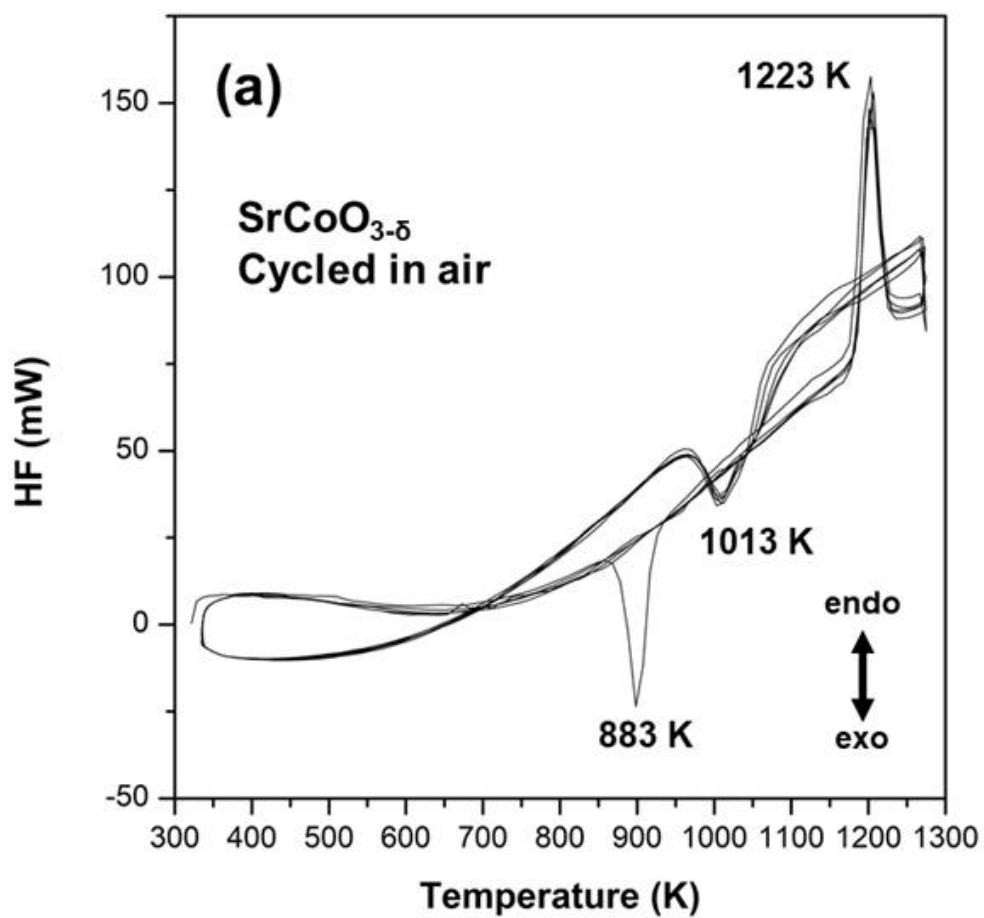
Figure 5. DSC curves of the SrCoO$_{3-\delta}$ sample a) five cycles, b) first cycle, and c) fifth cycle.

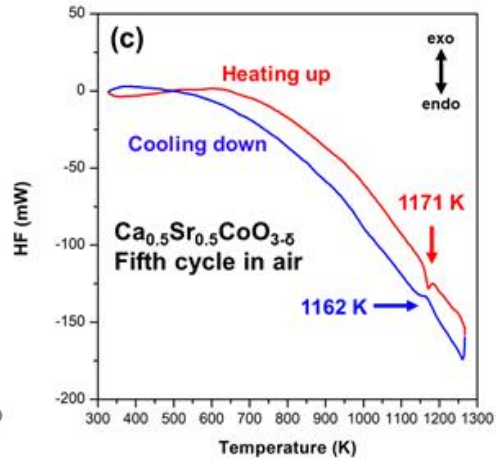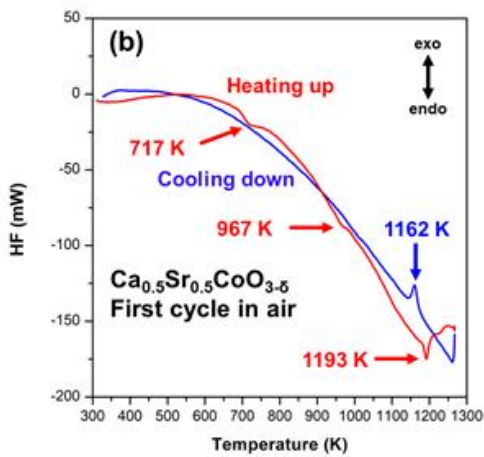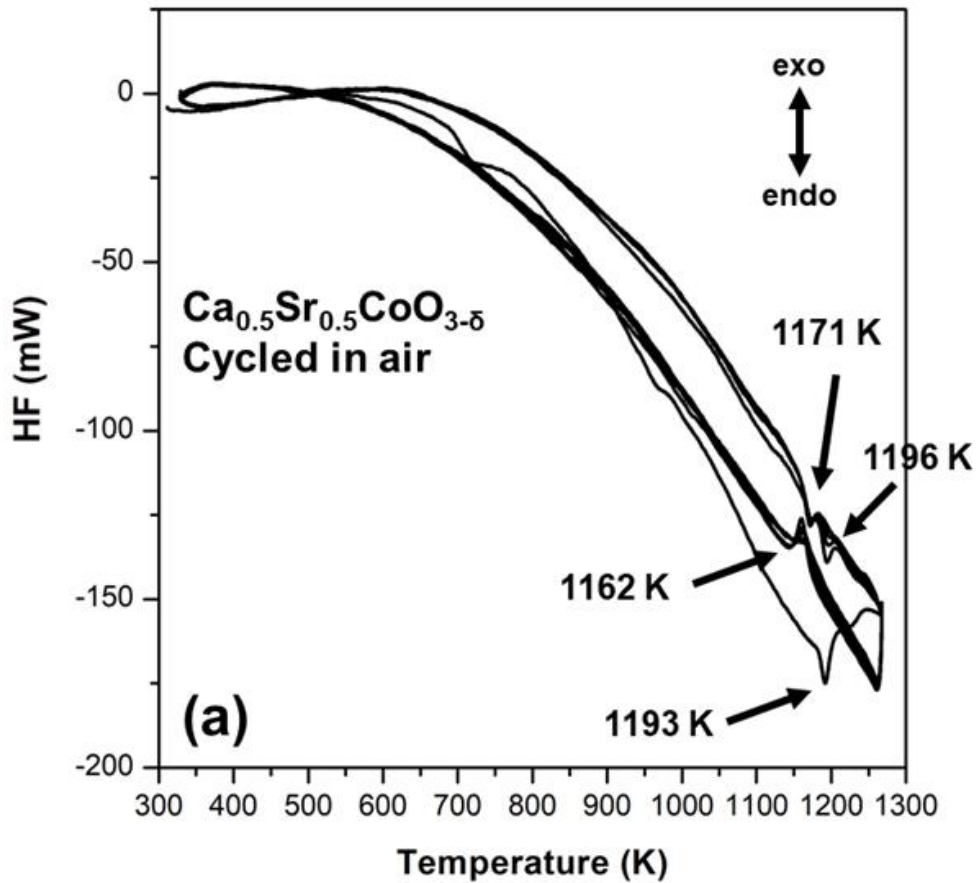**Figure 6.** DSC curves of the $Ca_{0.5}Sr_{0.5}CoO3-\delta$ sample a) five cycles, b) first cycle, and c) fifth cycle.

During the first heating, the CSCO sample experiences three reduction (Figure S4) endothermic processes (Figure 6b) centered at 717 K, 967 K, and 1193 K, respectively. The two first events proceed with no apparent structural transition (Figure 3 and Figure S6) at the resolution level of powder XRD. This fact suggests that those processes mainly involve slight oxygen losses and re-arrangement but retaining the brownmillerite structure. The third event corresponds to the B $\rightarrow$ C transition associated with a slight oxygen loss. In the first cooling, only one exothermic event is observed at 1162 K associated to the reversible C $\rightarrow$ B. In contrast, the processes at a lower temperature are irreversible as the oxygen gain, and material re-oxidation is only partial (Figure S4). Since the material suffers from a noticeable lack of cyclability, or at least its behavior is strongly limited by kinetical aspects, in both energy (Figure 6) and mass change (Figure 4b) terms, the compound $Ca_{0.5}Sr_{0.5}CoO_{3-\delta}$ must be discarded for thermochemical heat storage by thermochemical cycles.

On the contrary, as stated above, preliminary studies revealed that $SrCoO_{3-\delta}$ sample displays good cyclability during five consecutive cycles (Figures 4 and 5). Therefore, this material deserves further study as a potential candidate for the application.

Study of the absorbed and released heat by $SrCoO_{3-\delta}$ upon cycling. Long-term stability and cyclability of the SCO material have been studied for 30 consecutive heating-cooling cycles in air. The mass change and heat-flow along the whole experiment are shown in Figures 7a and 7b, respectively. The compound presents a reversible mass variation of around 1.6 % upon cycling, which is higher than the values reported in the literature for other perovskite-like materials,[41] making SCO a promising material. The DSC curves associated with the 30 cycles are depicted in Figure 7b. Except for the first cycle, the heat-flow is highly reversible upon cycling. Thus, the compound is stable not only from a compositional point of view, but also in energy terms.
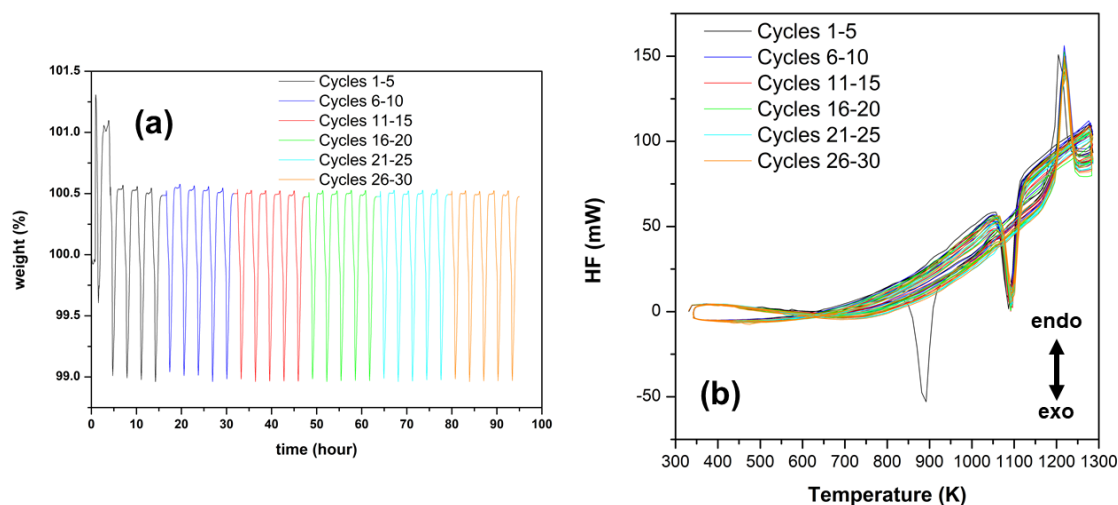
Figure 7. Mass change (a) and heat-flow (b) along upon cycling the SCO sample in air.

The integration of the endothermic peak at 1223 K and the exothermic one at 1013 K (Figures 5a and 7b) allows calculating the heat absorbed and released upon cycling. The values obtained for each consecutive cycle are summarized in Table 1. The difference observed in the heat absorbed during the first cycle is due to the sample transformations already discussed (Figures 2, 4, S3, and S5). The average heat absorbed from the second and successive cycles is ~ 104.1±0.06 J/g. The small value of the standard deviation confirms the good material reversibility and stability. Regarding the heat released, the average value is ~ 68.8±1.8 J/g. Another important aspect regarding the thermochemical heat storage application is the ratio between the heat released and absorbed upon cycling, the so-called exo/endo ratio. This is also included in Table 1 for $SrCoO_{3-\delta}$, and the average from the second and successive cycles is ~ 66.4±1.3 %.

It can be though that segregated Co_3O_4 may play a role in both oxygen (mass) loss/gain and energy stored/released upon cycling.[20] However, according to Eq. (4) the amount of segregated cobalt oxide is about 7% of the total mass; this means that assuming some 6% mass variation in the phase transformation from Co_3O_4 to CoO, the contribution of cobalt oxide to the total mass change observed is absolutely negligible.

Regarding energy storage, different values for the energy of the endothermic (reduction) and exothermic (oxidation) processes are reported for the system Co_3O_4/CoO depending on the

experimental conditions applied. To avoid any ambiguity, we have measured several DSC cycles of high purity commercial Co_3O_4 using the same conditions applied to characterize our materials (see the Experimental section). Figure S9 depicts the DSC curves in air of Co_3O_4 and $Sr_{0.5}CoO_{3-\delta}$ for comparison. By integration of the reduction and oxidation peaks the values of 12.4 J/g and 3.4 J/g are obtained for the reduction and oxidation, respectively. Using these values, the contribution of segregated cobalt oxide to the values in Table 1 will be no more than 10%. Besides, cobalt oxide presents poor cyclability, so its contribution will continuity decrease. This is a behavior totally different to what observed in Figure 7.

Table 1. Heat absorbed and released upon cycling $SrCoO_{3-\delta}$

| Cycle | Heat of the process (J/g) | | Ratio exo/endo (%) |
	Endothermic	Exothermic	
1	-90.0	66.6	74.0
2	-103.3	65.4	63.3
3	-104.1	67.0	64.4
4	-104.5	69.9	66.9
5	-103.9	67.5	65.0
6	-104.5	70.3	67.3
7	-104.1	69.8	67.1
8	-104.3	70.1	67.2
9	-104.2	71.2	68.3
10	-104.0	70.6	67.9
15	-104.5	70.0	66.9
20	-103.8	68.1	65.6
25	-104.2	69.5	66.7
30	-104.5	70.2	67.2

The two compounds reported in this study undergo reversible phase transition on heating/cooling in air. Nevertheless, they present noticeable differences depending on the nature of the phase transitions and their mechanisms. The $Ca_{0.5}Sr_{0.5}CoO_{3-\delta}$ perovskite can be reduced and re-oxidized in the temperature range 1162 K–1196 K, showing good reversibility upon cycling. However, the heat stored in these processes is very small, preventing its use for thermochemical energy storage. In this case, the structural transition occurs between the brownmillerite and cubic-perovskite. As shown in Figure 8, in both structures, the stacking sequence of layers AO3 (A = Ca and/or Sr) and cobalt-layers are similar. The main differences between these structures are the order of the oxygen vacancies and slight shifts of Co ions. In the brownmillerite phase the concentration of vacancies is lower, but they are ordered, whereas the large concentration of vacancies of anions in the perovskite induces disorder. Therefore, the B $\rightleftarrows$ C transition occurs with some oxygen loss/gain and a slight re-arrangement of light atoms such as oxygen; as a result, this transition is associated with a small amount of energy.
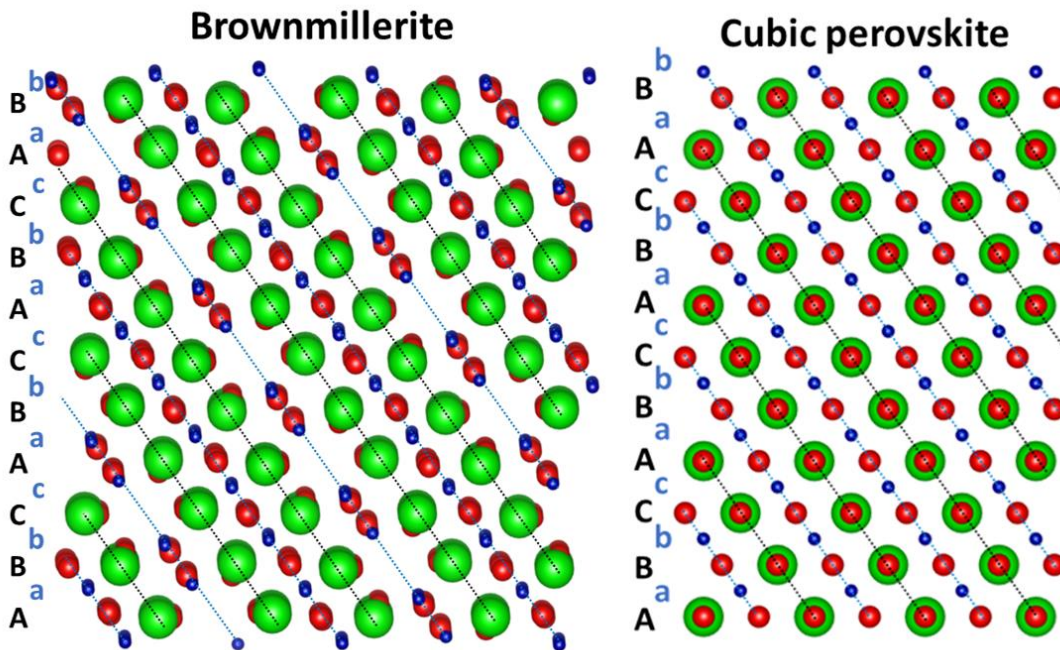
Figure 8. Schematic representation of the structures of brownmillerite (left panel) and cubic-perovskite (right panel), showing the stacking sequences of AO3-layers as (ABC) and Co-ions layers (abc) in both structures. Green large balls are A-ions (Sr and/or Ca in the title compounds), red balls represent oxygen, and small blue balls indicate Co-ions.

On the other hand, the $SrCoO_{3-\delta}$ perovskite can be reduced and re-oxidized in a temperature range between 1013 K–1123 K showing a reversible behavior along 30 consecutive cycles. In this case, the phase transition associated with the redox process is 2H $\rightleftarrows$ C, which involves larger structural changes than the B $\rightleftarrows$ C transition. Figure 9 depicts the atomic mechanism of this transition.[42,43] The stacking sequences of both AO3 and Co-ions layers are very different in these structures: (AB) and (aa) in the 2H-perovskite, and (ABC) and (abc) in the C-perovskite. Therefore, the phase transition 2H $\rightleftarrows$ C occurs with an extended atomic re-arrangement of all kinds of atoms. As sketched in Figure 9, a shear displacement of two AO3-layers blocks (large black arrows) combined with the displacement of some Co atoms (small blue arrows) transform the 2H-perovskite into a highly oxide defective C-perovskite. Since the transition involves a large number of atoms, including heavy metal ions, the energy absorbed/released by $SrCoO_{3-\delta}$ is much higher than by the Ca-substituted oxide.
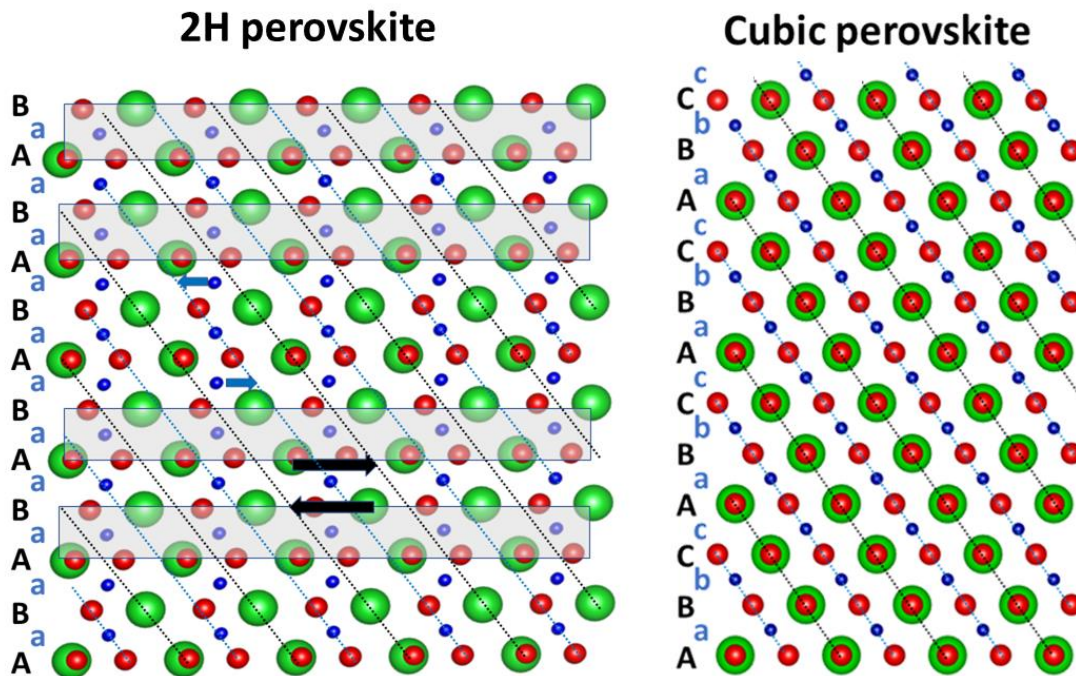
Figure 9. Schematic representation of the structures of 2H-perovskite (left panel) and cubic-perovskite (right panel), showing the stacking sequences of AO3-layers and Co-ions layers: in the former they are (AB) and (aa), whereas in the latter they are (ABC) and (abc). A shear mechanism of blocks shadowed in the figure, as indicated by the black arrows, combined with displacement of some Co-ions (small blue arrows) explains the phase transition. Green large balls are A-ions (Sr and/or Ca in the title compounds), red balls represent oxygen, and small blue balls indicate Co-ions.

Many perovskites continuously lose oxygen on heating in air (or inert atmosphere). This smooth reduction implies a continuous supply of small amounts of energy along the reaction. Therefore, a precise measurement of the enthalpy associated to reduction is not easy by conventional thermal analysis methods (such as DSC), in contrast to the enthalpy associated to first-order phase transitions (including structural ones) occurring at given thermodynamic conditions (pressure and

temperature). Hence, the thermochemical data on perovskite-like oxides necessary to assess their ability as TES materials are scarce. And very often, the published estimated values of the energy storage density for perovskites are obtained in very different conditions one from each other. In many studies, the reduction step of the thermochemical cycles is performed under inert atmosphere (Ar or N_2) or under dynamic vacuum at an arbitrary temperature, and the oxidation is conducted at an arbitrarily selected temperature under any convenient oxidizing atmosphere (oxygen, air, etc).[37] In our case, both reduction and oxidation processes are carried out in air. This being an advantage, it makes very difficult any comparison between our data and those reported in other studies.

Among the different thermochemical energy storage studies focused on materials with perovskite-type structure, it is worth highlighting the data reported for the oxides $Ba_xSr_{1-x}CoO_{3-\delta}$ (x= 0.3, 0.5 and 0.7).[24] The average values of heat absorbed and released in two cycles are as high as -174.0 and 169.2 J/g, respectively, for $Ba_{0.7}Sr_{0.3}CoO_{3-\delta}$. The values provided in this paper [24] are higher than those we obtain for $SrCoO_{3-\delta}$, but it seems that those data suffer from some inconsistencies. It must be noted that in the case of the oxides with x = 0.5 and 0.7, the reported ratio exo/endo is greater than 100 %, which is meaningless. The thermochemical energy stored by these materials is associated to redox reactions which involve modification of the amount of oxygen in the crystal lattice. Therefore, it is necessary to perform detailed structural and compositional studies on good samples of the starting material; besides, the thermal structure evolution must be known to determine their real capabilities as thermochemical storage materials. It is well established that very precise synthesis conditions must be applied to obtain pure samples of the solid solution $Ba_{1-x}Sr_xCoO_{3-\delta}$ ($0 \leq x \leq 1$), which present hexagonal perovskite structure and display several phase transitions on heating in different atmospheres.[44] Most likely, the high values endo and exo

energies reported by Gokon et al. [24] are related to phase transitions observed in this system, which deserves a more detailed study.

Zhang et al. [45] measured the enthalpy of oxidation of a sample of $SrCoO_{3-\delta}$ previously reduced (the reduction process is performed in Ar at 1223 K, whereas the oxidation is done at 873 K at a pO_2 = 0.2 atm); the value obtained is as low as 39.6 J/g. The authors associate this small value with the oxidation stage of the reaction sequence $SrCoO_{2.52} \rightarrow SrCoO_{2.19} \rightarrow SrCoO_{2.43}$. However, the pristine starting sample in this study seems to be not sufficiently pure, and a deeper compositional and structural study should be done to explain the results without any ambiguity.

To determine the efficiency of thermal storage devices for CSP plants,[46] not only the weight variation and the energy absorbed and released are important; the operational temperatures of the thermochemical-energy storage processes are also important. In general, reduction and oxidation take place at different temperatures. Thus, heat is stored and released at different temperatures, inducing thermal hysteresis. This is one of the main factors affecting the charge-discharge exergy efficiency, as these temperatures should be as close as possible, which would result in higher exergy efficiencies, as given by Equation 5:

$$\eta_{ex} = \frac{Q_{out}\left(1-\frac{T_C}{T_{out}}\right)}{Q_{in}\left(1-\frac{T_C}{T_{in}}\right)} \qquad (5)$$

Where T_{in} and T_{out} are the temperatures at which reduction and oxidation processes take place, respectively, whereas T_c is the cold reservoir temperature (298 K).[46] Table 2 summarizes the operational temperatures, the shift between reduction and oxidation temperatures ($\Delta T_{hysteresis}$), and the values of η_{ex} calculated over the 30 consecutive cycles, measured for SCO. Both operating temperatures, the reduction one (i.e., the temperature at which maximum oxygen release rates are

reached) and the oxidation one (i.e., the temperature at which maximum oxygen intake rates are reached), remain constant for consecutive cycles, confirming the good stability and cyclability of this material. Additionally, the shift between reduction and oxidation temperatures ($\Delta T_{hysteresis}$) is similar to the values reported for other metal oxides, such as those presented in Table 3, commonly proposed in the literature for the application.[5, 38,39,47,48] The exergy efficiencies are almost constant upon cycling from the second cycle, with an average value of 63.9±1.2 %. Note in Table 3 the lack of information for perovskite-like oxides and the particular experimental conditions used (fixed reduction and oxidation temperatures) to estimate the reported data.[24,41] It is obvious that perovskite oxides, in particular those hexagonal perovskites which undergo a phase transition to a cubic phase on heating, deserve more studies to assess their real capabilities for thermochemical storage.

Additionally, the operational temperatures must be compatible with the working conditions of other parts of the CSP plants, such as the solar concentrator (which must concentrate the solar radiation to reach the required temperatures) and the receiver (where reactions take place). Assuming that the solar reactor is a perfectly insulated black-body receiver, the absorption efficiency is given by Equation [6]:

$$\eta_{abs} = 1 - \frac{(\theta\, T_{reactor}^4)}{IC} \tag{6}$$

where θ is the Stefan–Boltzmann constant (5.67·10-11 KW/m2·K4); $T_{reactor}$ is the solar reactor temperature (T_{in}); I is the direct-normal solar irradiation (taken as 1 KW·m^2); and C is the concentration ratio which is defined as the solar radiative flux normalized to 1 kW/m^2 and is usually expressed in "suns" units.[49] Table 4 collects the absorption efficiency for the oxide $SrCoO_{3-\delta}$ and other materials widely studied as a function of C.

Table 2. Operational temperatures, temperature gap, and exergy efficiency for SrCoO$_{3-\delta}$ upon cycling.

Cycle	T_{in} (K)	T_{out} (K)	$\Delta T_{hysteresis}$ (K)	η_{ex} (%)
1				70.5
2				60.3
3				61.3
4				63.8
5				61.9
6				64.1
7				63.9
	1223	1013	210	
8				64.1
9				65.1
10				64.7
15				63.8
20				62.5
25				63.6
30				64.0

The theoretical solar absorption efficiency calculated with SCO is higher than the values obtained with other metals oxides such as Co$_3$O$_4$ or Mn$_2$O$_3$, and similar or better than those reported for other perovskites.

Table 3. Exergy efficiency for different metal-oxygen systems reported in the literature.*

Material	T_{in} (K)	T_{out} (K)	ΔT (K)	η_{ex} (%)
Co_3O_4/CoO	1273	873	400	71.0
Mn_2O_3/Mn_3O_4	1273	823	450	40.8
BaO_2/BaO	993	853	140	37.9
$Ba_{0.3}Sr_{0.7}CoO_{3-\delta}$	1183	1023	160	74.4
$Ba_{0.5}Sr_{0.5}CoO_{3-\delta}$	1183	1073	110	102.3
$Ba_{0.7}Sr_{0.3}CoO_{3-\delta}$	1203	1093	110	99.4
$SrMnO_{3-\delta}$	1423	873	550	--
$SrCoO_{3-\delta}$ (this work)	1223	1013	210	63.9

*Data taken from [1-4]

Table 4. Solar absorption efficiencies as a function of C for different metal-oxygen systems.*

Material	η_{abs}(%) as a function of C (suns)				
	C=1000	C=2000	C=3000	C=4000	C=5000
Co_3O_4/CoO	0.85	0.93	0.95	0.96	0.97
Mn_2O_3/Mn_3O_4	0.85	0.93	0.95	0.96	0.97
BaO_2/BaO	0.94	0.97	0.98	0.99	0.99
$Ba_{0.3}Sr_{0.7}CoO_{3-\delta}$	0.88	0.94	0.96	0.97	0.98
$Ba_{0.5}Sr_{0.5}CoO_{3-\delta}$	0.88	0.94	0.96	0.97	0.98
$Ba_{0.7}Sr_{0.3}CoO_{3-\delta}$	0.88	0.94	0.96	0.97	0.98
$SrMnO_{3-\delta}$	0.77	0.88	0.94	0.95	0.96
$SrCoO_{3-\delta}$ (this work)	0.88	0.94	0.96	0.97	0.98

*Calculated using data from [1, 3-5]

CONCLUSIONS

The two compounds reported in this study $SrCoO_{3-\delta}$ and $Ca_{0.5}Sr_{0.5}CoO_{3-\delta}$ can be easily reduced and re-oxidized under air flow at intermediate temperatures. Furthermore, these perovskites undergo structural transitions associated with redox processes, the combination of these two properties is clearly beneficial for thermochemical energy storage applications as it results in significantly high efficiency. Nevertheless, they present noticeable differences depending on the nature of the phase transitions and their mechanisms. The $Ca_{0.5}Sr_{0.5}CoO_{3-\delta}$ oxide experiences a structural transition between the brownmillerite and cubic-perovskite; in both structures, the stacking sequence of layers AO3 (A = Ca and/or Sr) and cobalt-layers are similar the B $\rightleftarrows$ C transition occurs with some oxygen loss/gain and a slight re-arrangement of light atoms such as oxygen; as a result, this transition is associated with a small amount of energy.

On the contrary the reduction/ re-oxidizion of $SrCoO_{3-\delta}$ perovskite is associated to a phase transition 2H $\rightleftarrows$ C, which involves larger structural changes than the B $\rightleftarrows$ C transition; the former occurs with an extended atomic re-arrangement of a large number of atoms, including heavy metal ions, as a result the energy absorbed/released by $SrCoO_{3-\delta}$ is much higher than by the Ca-substituted oxide.

The perovskite $SrCoO_{3-\delta}$ is a promising material for thermochemical energy storage because the values of energy absorbed and released, as well as the exergy efficiency, are comparable to those reported in the literature for other metal-oxygen systems, the reduction/oxidation processes and the associated phase transition is highly reversible and the whole redox cycle is easily performed in air.

The present study opens the field of thermochemical energy storage to other hexagonal perovskites, which display reversible phase transitions coupled with redox processes associated to gain/loss of oxygen.

ASSOCIATED CONTENT

Supporting Information available

X-ray diffraction patterns, structural parameters, and DSC data in air.

AUTHOR INFORMATION

Corresponding Author

* M. Teresa Azcondo, Phone (+34) 91 372 47 57, E-mail: azcondo@ceu.es
* Raúl Sanz, Phone (+34) 91 488 8093, E-mail: raul.sanz@urjc.es

Author Contributions

The manuscript was written through contributions of all authors (†, ǀ, ‡, ⁂). All authors have given approval to the final version of the manuscript.

Notes

The authors declare no competing financial interest.

ABBREVIATIONS

CSP concentrated solar power, TES thermal energy storage, PCMs phase-change materials,

TCES thermochemical energy storage, SCO $SrCoO_{3-\delta}$, CSCO $Ca_{0.5}Sr_{0.5}CoO_{3-\delta}$, B brownmillerite,

C cubic, H hexagonal, XRD X-ray diffraction, RT room temperature, HREM high-resolution

electron microscopy, TGA thermogravimetric analysis.

REFERENCES

1. Bilgen S. Structure and environmental impact of global energy consumption. Renewable & Sustainable Energy Reviews. 2014;38:890-902.
2. Agrawal R, Mallapragada DS. Chemical Engineering in a Solar Energy-Driven Sustainable Future. Aiche Journal. 2010;56(11):2762-8.
3. Azzuni A, Breyer C. Energy security and energy storage technologies. In: Droege P, editor. 12th International Renewable Energy Storage Conference, Ires 20182018. p. 237-58.
4. Child M, Bogdanov D, Breyer C. The role of storage technologies for the transition to a 100% renewable energy system in Europe. In: Droege P, editor. 12th International Renewable Energy Storage Conference, Ires 20182018. p. 44-60.
5. Pardo P, Deydier A, Anxionnaz-Minvielle Z, Rouge S, Cabassud M, Cognet P. A review on high temperature thermochemical heat energy storage. Renewable & Sustainable Energy Reviews. 2014;32:591-610.
6. Chen X, Zhang Z, Qi C, Ling X, Peng H. State of the art on the high-temperature thermochemical energy storage systems. Energy Conversion and Management. 2018;177:792-815.
7. Breidenbach N, Martin C, Jockenhoefer H, Bauer T. Thermal Energy Storage In Molten Salts: Overview Of Novel Concepts And The DLR Test Facility TESIS. In: Droege P, editor. 10th International Renewable Energy Storage Conference, Ires 20162016. p. 120-9.
8. Niedermeier K, Marocco L, Flesch J, Mohan G, Coventry J, Wetzel T. Performance of molten sodium vs. molten salts in a packed bed thermal energy storage. Applied Thermal Engineering. 2018;141:368-77.
9. Sarvghad M, Steinberg TA, Will G. Corrosion of stainless steel 316 in eutectic molten salts for thermal energy storage. Solar Energy. 2018;172:198-203.

10. Berardi U, Soudian S. Experimental investigation of latent heat thermal energy storage using PCMs with different melting temperatures for building retrofit. Energy and Buildings. 2019;185:180-95.

11. Khare S, Dell'Amico M, Knight C, McGarry S. Selection of materials for high temperature sensible energy storage. Solar Energy Materials and Solar Cells. 2013;115:114-22.

12. Zhao P, Yue Q, He H, Gao B, Wang Y, Li Q. Study on phase diagram of fatty acids mixtures to determine eutectic temperatures and the corresponding mixing proportions. Applied Energy. 2014;115:483-90.

13. Huang X, Zhu C, Lin Y, Fang G. Thermal properties and applications of microencapsulated PCM for thermal energy storage: A review. Applied Thermal Engineering. 2019;147:841-55.

14. Prieto C, Rodriguez A, Patino D, Cabeza LF. Thermal energy storage evaluation in direct steam generation solar plants. Solar Energy. 2018;159:501-9.

15. Malley-Ernewein A, Lorente S. Constructal design of thermochemical energy storage. International Journal of Heat and Mass Transfer. 2019;130:1299-306.

16. Karagiannakis G, Pagkoura C, Halevas E, Baltzopoulou P, Konstandopoulos AG. Cobalt/cobaltous oxide based honeycombs for thermochemical heat storage in future concentrated solar power installations: Multi-cyclic assessment and semi-quantitative heat effects estimations. Solar Energy. 2016;133:394-407.

17. Schaube F, Woerner A, Tamme R. High Temperature Thermochemical Heat Storage for Concentrated Solar Power Using Gas-Solid Reactions. Journal of Solar Energy Engineering-Transactions of the Asme. 2011;133(3).

18. Agrafiotis C, Roeb M, Schmuecker M, Sattler C. Exploitation of thermochemical cycles based on solid oxide redox systems for thermochemical storage of solar heat. Part 1: Testing of cobalt oxide-based powders. Solar Energy. 2014;102:189-211.

19. Bayon A, Bader R, Jafarian M, Fedunik-Hofman L, Sun Y, Hinkley J, Miller S, Lipiński W., Techno-economic assessment of solid-gas thermochemical energy storage systems for solar thermal power applications. Energy. 2018;149:473-84.

20. Carrillo AJ, Moya J, Bayon A, Jana P, de la Pena O'Shea VA, Romero M, Gonzalez Aguilar J, Serrano D.P., Pizarro P., Coronado J. M. Thermochemical energy storage at high temperature via redox cycles of Mn and Co oxides: Pure oxides versus mixed ones. Solar Energy Materials and Solar Cells. 2014;123:47-57.

21. Wokon, M., Block, T., Nicolai, S., Linder M., Schmücker, M. Thermodynamic and kinetic investigation of a technical grade manganese-iron binary oxide for thermochemical energy storage Solar Energy 153, 471-485, (2017)

22. Babiniec SM, Coker EN, Miller JE, Ambrosini A. Investigation of LaxSr1-xCoyM1-yO3-δ (M = Mn, Fe) perovskite materials as thermochemical energy storage media. Solar Energy. 2015;118:451-9.

23. Albrecht KJ, Jackson GS, Braun RJ. Thermodynamically consistent modeling of redox-stable perovskite oxides for thermochemical energy conversion and storage. Applied Energy. 2016;165:285-96.

24. Gokon N, Yawata T, Bellan S, Kodama T, Cho H-S. Thermochemical behavior of perovskite oxides based on LaxSr1-x(Mn, Fe, Co)O3-δ and BaySr1-yCoO3-δ redox system for thermochemical energy storage at high temperatures. Energy. 2019;171:971-80.

25. Imponenti L, Albrecht KJ, Kharait R, Sanders MD, Jackson GS. Redox cycles with doped calcium manganites for thermochemical energy storage to 1000°C. Appl. Energ., 2018;230:1-18.

26. Chen X, Kubota M, Yamashita S, Kita H. Investigation of Sr-based perovskites for redox-type thermochemical energy storage media at medium-high temperature. J. Energy Storage, 2021;38:102501.

27. Jin F, Xu C, Yu H, Xia X, Ye F, Li X, Du X, Yang Y. CaCo0.05Mn0.95O3-δ: A Promising Perovskite Solid Solution for Solar Thermochemical Energy Storage. ACS Appl. Mater. Interfaces, 2021;13(3):3856-66.

28. Vieten J, Bulfin B, Senholdt M, Roeb M, Sattler C, Schmuecker M. Redox thermodynamics and phase composition in the system SrFeO3-δ - SrMnO3-δ. Solid State Ionics. 2017;308:149-55.

29. Jain SR, Adiga KC, Verneker VRP. A new approach to thermochemical calculations of condensed fuel-oxidizer mixtures. Combustion and Flame. 1981;40(1):71-9.

30. Rodríguez-Carvajal J. Recent advances in magnetic structure determination by neutron powder diffraction. Physica B: Condensed Matter. 1993;192(1):55-69.

31. Le Bail A. Whole powder pattern decomposition methods and applications: A retrospection. Powder Diffraction. 2005;20(4):316-26.

32. de la Calle C, Alonso JA, Fernandez-Diaz MT. Polymorphism of Ba(1-x)Sr(x)CoO(3-δ) (0 <= x <= 1) perovskites: A thermal and structural study by neutron diffraction. Zeitschrift Fur Naturforschung Section B-a Journal of Chemical Sciences. 2008;63(6):647-54.

33. Harrison WTA, Hegwood SL, Jacobson AJ. A powder neutron-diffraction determination of the structure of Sr6Co5O15, formerly described as the low-temperature hexagonal form of srcoo3-x. Journal of the Chemical Society-Chemical Communications. 1995(19):1953-4.

34. Takeda Y, Kanno R, Takada T, Yamamoto O, Takano M, Bando Y. Phase relation and oxygen-non-stoichiometry of perovskite-like compound SrCoOx (2.29 less-than x less-than 2.80). Zeitschrift Fur Anorganische Und Allgemeine Chemie. 1986;541(9-10):259-70.

35. Sun J, Li G, Li Z, You L, Lin J. Crystal growth and structure determination of oxygen-deficient Sr6Co5O15. Inorganic Chemistry. 2006;45(20):8394-402.

36. Miura N, Murae H, Kusaba H, Tamaki J, Sakai G, Yamazoe N. Oxygen permeability and phase transformation of Sr0.9Ca0.1CoO2.5+δ. Journal of the Electrochemical Society. 1999;146(7):2581-6.

37. Sekhar BS, Muthukumar P, Saikia R. Tests on a metal hydride based thermal energy storage system. International Journal of Hydrogen Energy. 2012;37(4):3818-24.

38. Agrafiotis C, Roeb M, Sattler C. Exploitation of thermochemical cycles based on solid oxide redox systems for thermochemical storage of solar heat. Part 4: Screening of oxides for use in cascaded thermochemical storage concepts. Solar Energy. 2016;139:695-710.

39. Wu S, Zhou C, Doroodchi E, Nellore R, Moghtaderi B. A review on high-temperature thermochemical energy storage based on metal oxides redox cycle. Energy Conversion and Management. 2018;168:421-53.

40. Orfila M, Linares M, Molina R, Angel Botas J, Marugan J, Sanz R. Thermochemical hydrogen production using manganese cobalt spinels as redox materials. International Journal of Hydrogen Energy. 2017;42(19):13532-43.

41. Andre L, Abanades S. Investigation of metal oxides, mixed oxides, perovskites and alkaline earth carbonates/hydroxides as suitable candidate materials for high-temperature thermochemical energy storage using reversible solid-gas reactions. Materials Today Energy. 2018;10:48-61.

42. Arnold M, Gesing TM, Martynczuk J, Feldhoff A. Correlation of the formation and the decomposition process of the BSCF perovskite at intermediate temperatures. Chemistry of Materials. 2008;20(18):5851-8.

43. Cao S-G, Li Y, Wu H-H, Wang J, Huang B, Zhang T-Y. Stress-Induced Cubic-to-Hexagonal Phase Transformation in Perovskite Nanothin Films. Nano Letters. 2017;17(8):5148-55.

44. Calle C, Alonso J, Fernández-Díaz M. Polymorphism of Ba1–xSrxCoO3–δ (0≤ x≤ 1) Perovskites: A Thermal and Structural Study by Neutron Diffraction. Zeitschrift fur Naturforschung - Section B Journal of Chemical Sciences. 2008;63:647-56.

45. Zhang Z, Andre L, Abanades S. Experimental assessment of oxygen exchange capacity and thermochemical redox cycle behavior of Ba and Sr series perovskites for solar energy storage. Solar Energy. 2016;134:494-502.

46. Weinstein LA, Loomis J, Bhatia B, Bierman DM, Wang EN, Chen G. Concentrating Solar Power. Chemical Reviews. 2015;115(23):12797-838.

47. Yan T, Wang RZ, Li TX, Wang LW, Fred IT. A review of promising candidate reactions for chemical heat storage. Renewable & Sustainable Energy Reviews. 2015;43:13-31.

48. Bauer T. Chapter 1 - Fundamentals of high-temperature thermal energy storage, transfer, and conversion. In: Datas A, editor. Ultra-High Temperature Thermal Energy Storage, Transfer and Conversion: Woodhead Publishing; 2021. p. 1-34.

49. Parrott JE. Choice of an equivalent black-body solar temperature. Solar Energy. 1993; 51(3):195.